Computational and Structural Biotechnology Journal 21 (2023) 4634–4646

Contents lists available at ScienceDirect

Computational and Structural Biotechnology Journal

journal homepage: www.elsevier.com/locate/csbj

Research article

Enzyme-constrained metabolic model and *in silico* metabolic engineering of *Clostridium ljungdahlii* for the development of sustainable production processes

Antonio Caivano [a], Wouter van Winden [b], Giuliano Dragone [a], Solange I. Mussatto [a,*]

[a] Department of Biotechnology and Biomedicine, Technical University of Denmark, Søltofts Plads, Building 223, 2800, Kongens Lyngby, Denmark
[b] DSM-Firmenich Science & Research - Bioprocess Innovation, Rosalind Franklin Biotechnology Center, Alexander Fleminglaan 1, 2613 AX, Delft, the Netherlands

ARTICLE INFO

Keywords:
Genome-scale model
Acetogenic bacteria
CO2 fixation
Flux balance analysis
OptKnock
Metabolic engineering

ABSTRACT

Constraint-based genome-scale models (GEMs) of microorganisms provide a powerful tool for predicting and analyzing microbial phenotypes as well as for understanding how these are affected by genetic and environmental perturbations. Recently, MATLAB and Python-based tools have been developed to incorporate enzymatic constraints into GEMs. These constraints enhance phenotype predictions by accounting for the enzyme cost of catalyzed model's reactions, thereby reducing the space of possible metabolic flux distributions. In this study, enzymatic constraints were added to an existing GEM of *Clostridium ljungdahlii*, a model acetogenic bacterium, by including its enzyme turnover numbers (k_{cat}s) and molecular masses, using the Python-based AutoPACMEN approach. When compared to the metabolic model iHN637, the enzyme cost-constrained model (ec_iHN637) obtained in our study showed an improved predictive ability of growth rate and product profile. The model ec_iHN637 was then employed to perform *in silico* metabolic engineering of *C. ljungdahlii*, by using the OptKnock computational framework to identify knockouts to enhance the production of desired fermentation products. The *in silico* metabolic engineering was geared towards increasing the production of fermentation products by *C. ljungdahlii*, with a focus on the utilization of synthesis gas and CO_2. This resulted in different engineering strategies for overproduction of valuable metabolites under different feeding conditions, without redundant knockouts for different products. Importantly, the results of the *in silico* engineering results indicated that the mixotrophic growth of *C. ljungdahlii* is a promising approach to coupling improved cell growth and acetate and ethanol productivity with net CO_2 fixation.

1. Introduction

The widespread adverse impacts of human caused climate change has made necessary a global effort for accelerating the reduction of anthropogenic greenhouse gas emissions [1]. As the main greenhouse emitted gas, CO_2 reduction is the main target of most of the strategies to counteract climate warming; the main processes for the capture of CO_2 typically are grouped as carbon capture and storage (CCS) and carbon capture and utilization (CCU) strategies, depending on the fate of the CO_2 [2]. In CCU strategies hold great potential as recaptured CO_2 is utilized as a feedstock for chemical, biochemical, and electrochemical processes to produce materials and chemicals. This approach can play a significant role in the development of a circular economy, allowing potential carbon-negative products. In biologically mediated CCU, biological systems are utilized to capture and utilize CO_2 present at the emission source, or in the atmosphere, to be introduced in the metabolism of autotrophic bacteria, algae, or archaea [3]. Among autotrophic microorganisms, acetogenic bacteria, or acetogens are particularly interesting for potential industrial applications, employing an energetically efficient CO_2 fixating pathway, the reductive acetyl-CoA pathway, or Wood-Ljungdahl pathway (WLP)[4], [5]. In this pathway, 2 moles of CO_2 are converted to one mole of acetyl-CoA, utilizing H_2 as an electron donor[6]. The acetyl-CoA is then typically converted to acetic acid through phosphotransacetylase and acetate kinase, allowing to recover one mole of ATP per mole of acetic acid produced by phosphorylation at the substrate level [6]. Despite the promising potential of these microorganisms for industrial applications, their use has been hindered by their slow growth and low productivity when grown autotrophically,

* Corresponding author.
E-mail addresses: solangemussatto@hotmail.com, smussatto@dtu.dk (S.I. Mussatto).

https://doi.org/10.1016/j.csbj.2023.09.015
Received 15 June 2023; Received in revised form 13 September 2023; Accepted 13 September 2023
Available online 15 September 2023

particularly without the presence of CO. Until now, Lanzatech has been the only company developing a gas fermentation process with acetogens reaching commercial scale, successfully producing ethanol from syngas fermentation [7]. However, CO-rich syngas fermentation results in CO_2 emissions, coming from the oxidation of CO to CO_2; recently, a breakthrough has been described in a publication reporting the development of a gas fermentation process by an engineered *Clostridium autoethanogenum* strain, resulting in carbon-negative production of acetone and isopropanol [8].

Clostridium ljungdahlii is one of the most studied acetogen, known for its ability to convert different gaseous substrates, CO_2, H_2, and CO [9] through the Wood-Ljungdahl pathway, making it a promising candidate for conversion of synthesis gas into valuable chemicals. Moreover, *C. ljungdahlii* has been proven to be able to grow mixotrophically when fed with fructose, reconverting the CO_2-produced glycolysis through the Wood-Ljungdahl pathway [10]. Supplementation of an organic carbon source, resulting in a mixotrophic growth, is an interesting approach to boost the growth and productivity of acetogens, typically low during autotrophic growth, particularly in the case of a syngas composition poor in CO [11], [12]. Moreover, if enough H_2 is supplemented in the gas phase during mixotrophic growth, fixation of exogenous CO_2, not produced in glycolysis, is possible [10,13].

Native products of *C. ljungdahlii* are mainly acetic acid (HAc) and ethanol (EtOH) with the possibility to also produce small amounts of 2,3-butanediol (BDO) and lactic acid (LAc) [9,11,14]. Moreover, many attempts to broaden the product range of this specie have been performed over the last years, by insertion of heterologous biosynthetic pathways [15], to produce acetone, isopropanol, butyrate, butanol, and many other valuable chemicals. Industrial utilization of strains engineered for the production of longer chains and reduced chemicals may be strongly affected by the reduced growth rate caused by the energetic burden coming from the production of these products.

Genome-scale models (GEM) are mathematical representations of a metabolic network of a microorganism, reconstructed from the genome annotation of the microbe, utilizing a gene-protein-reaction stoichiometry association [16]. By utilizing computational tools such as Flux Balance Analysis (FBA), and Flux Variability Analysis (FVA), it is possible to constraint the uptake of nutrients and compute the outputs of the cell (growth rate and metabolites secretion) by maximizing an objective function, usually biomass production, under the hypothesis that this is the main biological objective of the microorganism [17]. The stoichiometries of the model's reactions, ensuring to maintain closed mass balances, impose a constraint on the fluxes of metabolites in the cell's metabolic network, allowing to identify a space of fluxes distributions allowing growth of the cell. Through optimization by FBA, the optimal flux distribution for maximization (or minimization) of the objective function is found [17]. Among the many utilizations of genome-scale models, there is the possibility to identify optimal genetic manipulations to produce a desired metabolite, by simulations of the growth of the strains in case of knock-out, additions of heterologous pathways, up- or down-regulation of gene expressions [18].

In the last decade, many strategies have been developed to improve the accuracy of metabolic models in the simulations of microbial growth. These strategies aim at including providing additional constraints to the model, such as thermodynamic, enzymatic, or kinetic constraints, in order to reduce the space of possible fluxes and improve the predictive ability of the model [19]. The introduction of additional constraints allows a better description of the microorganisms' physiology, accounting for other biological processes inside the cell, other than the sole network of metabolic reactions [19]. In the approach defined as Metabolic and gene Expression models (ME-models), genome-scale models are integrated with reactions accounting for macromolecular processes such as protein synthesis and transcriptional regulation, allowing to accurately predict gene expression levels and predict the maximum feasible growth rate without explicit constraining the substrate uptake rates [20,21]. Models constructed taking into account reaction kinetics can reach a very high fidelity of metabolic fluxes predictions, and successfully predict cell growth in a dynamic environment, accounting for the changes in nutrients and metabolite concentrations in complex environments [22,23]. A strong limitation in these approaches is the great amount of specific biological information needed for the parametrization of the models, which is not available for most microorganisms. Moreover, the computational effort required for the simulating growth of the microbe can be extremely challenging, due to the presence of non-linear expressions and processes taking place at radically different time scales [24].

The addition of constraints on the total amount of enzymes in the cell, following strategies such as MOMENT [25], short MOMENT [26], and GECKO [27] and ECMpy [28] has also the potential to increase the predictive ability of the simulated growth of the microorganism, utilizing readily available data as turnover rates (k_{cat}) and molecular weights (MW), without resulting in computationally demanding models, and allowing to utilize linear programming tools as for metabolic-only models.

The use of computational tools for synthetic biology may offer the possibility to better understand acetogens' metabolism, and guide towards possible metabolic engineering strategies to transform them into production hosts. A metabolic model was published in 2013 for *C. ljungdahlii* [29], represented the first genome-scale model available for an acetogenic bacterium, allowing to characterize the nitrate reduction pathway of this strain and clarify the role of flavin-based electron bifurcation. A ME model published in 2019 then allowed to describe the overflow metabolism of *C. ljungdahlii*, predicted gene expression of the bacterium in different conditions, and predicted the positive effect of Nickel availability on the growth rate [30].

The objective of the present study was to generate an enzyme-constrained model of *C. ljungdahlii*, by adding constraints on the total allocation of metabolic enzymes to the original model published by Nagarajan et al. [29], with the goal of improving its predictive capability. The performance of the model was evaluated using *in vivo* data sourced from both the existing literature and generated in our lab from the cultivation of the strain under mixotrophic conditions. Subsequently, the generated model was employed to predict optimal metabolic engineering strategies for enhancing the production of metabolites of interest under two different growth scenarios. The first scenario considered was syngas fermentation, which has been the most explored application of the strain. The second scenario was mixotrophic growth, which has recently been proposed as a potential strategy to overcome the energetic limitations in the growth of acetogenic bacteria [31,32].

2. Materials and methods

2.1. Addition of annotations to the original model

The *C. ljungdahlii* DSM 13528 metabolic model iHN637 [29] was used as the initial model for the construction of the enzyme-constrained model of the acetogen following the AutoPACMEN method [26]. The SBML (XML) file of the model iHN637 was downloaded from the BiGG Models [33] database. The model iHN637 has 698 metabolites, 785 reactions, and 637 genes; the report generated by the testing with MEMOTE [34] evidenced an overall high quality of the model, having a total score of 90%. The benchmark provided by MEMOTE is based on the consistency of the model and the quality of annotations. The very high consistency score (Fig. 1) indicates that mass and charge are well balanced, while the low score for gene annotations is because gene annotations are present only for the NCBI database. Before proceeding with the addition of the enzyme constraints, it was needed to update the model with the addition of UniProt IDs annotations and missing EC numbers, as these annotations are used in the AutoPACMEN workflow to retrieve the molecular weights of enzymes and the turnover numbers (k_{cat}) of reactions.

Gene annotations of UniProt IDs were added to the iHN637 model by

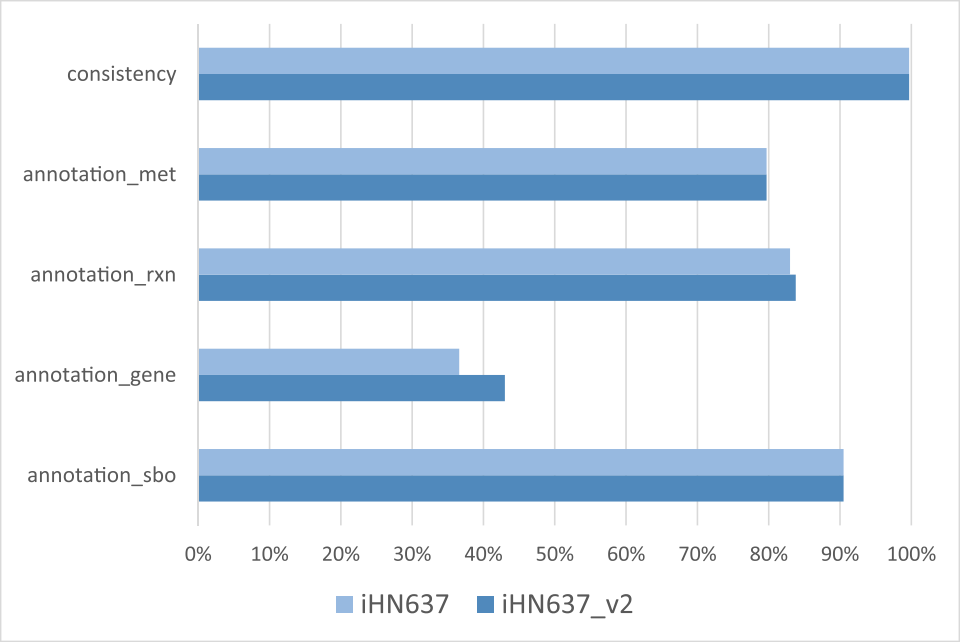

Fig. 1. Model scores by MEMOTE. Score for each model category evaluated by MEMOTE in the original model (iHN637) and the updated version (iHN637_v2).

using the UniProt ID Mapping tool on the UniProt website [35]. The 670 GI numbers (ncbigi gene annotation) provided in the original model were mapped to 1096 results, indicating a non-bijective correspondence between GI numbers and UniProt IDs, as some GI numbers were associated to multiple UniProt IDs belonging to different strains. Addition of the Uniprot IDs annotations increased the score for gene annotations from 36.6% to 43%; the score remained low as it is calculated considering also gene annotations for other databases; for the scope of the study, addition of Uniprot IDs was sufficient for the successive steps of the workflow.

The MEMOTE report indicated that 71% of the reactions in the model were assigned EC numbers (ec-code), while 228 reactions were not annotated. Most of these unannotated reactions were metabolite exchange reactions, typically not associated with EC numbers [36]. However, some of the reactions lacking the EC number were enzyme-catalyzed reactions, and for these, a manual search was conducted on the BRENDA Enzyme Database [37] to identify the corresponding EC number. The addition of the EC_numbers slightly increased the score for reaction annotations.

The retrieved UniProt IDs and the missing EC numbers were added to the XML file, and the updated model was analyzed by MEMOTE, to have a comprehensive overview and compare with the original version.

2.2. Background of short MOMENT (sMOMENT) model construction

Standard metabolic models are defined by a stoichiometric matrix, where each column corresponds to a reaction and each row corresponds to a metabolite, and a flux vector under steady state mass balance [17]:

$$\boldsymbol{Sv} = 0 \tag{1}$$

where each flux is constrained by a lower and upper bound:

$$\alpha_i \leq v_i \leq \beta_i \tag{1}$$

The short MOMENT method is characterized by the addition to the stoichiometric matrix of a pseudo metabolite (*i.e.* an additional row), containing the enzymatic cost (c) of each reaction, which for each reaction i was calculated as:

$$c_i = -\frac{MW_i}{k_{cat,i}} \tag{3}$$

A pseudo reaction is also added as a new column of the matrix, whose coefficients are 0 for all the metabolites except for thepseudo metabolite pool, for which it is 1.

The associated flux of this pseudo reaction was then constrained by an upper bond, the protein pool P, measuring the upper limit of metabolic enzymes mass in the cell [26]. The model, thus, was constrained allowing only a limited maximum mass of enzymes in the cell, which could be directly determined experimentally or derived by fitting experimental growth data to simulation results.

2.3. Generation of enzyme-constrained model

After the model update, it was possible to proceed with application of AutoPACMEN workflow for the generation of the enzyme-constrained model [26]. The AutoPACMEN package was downloaded from GitHub and installed, then the steps indicated by the authors were followed with few modifications for the addition of enzyme constraints:

1. The BiGG metabolite text file was downloaded from the BiGG website [33] and converted to the JSON format.
2. The BRENDA database text file was downloaded from the BRENDA Enzyme database website [37] and converted to the JSON format.
3. The BRENDA JSON file was parsed to retrieve the EC numbers present in the updated model; the associated k_{cat} was then saved into a new JSON file.
4. All the EC numbers in the model were searched in the SABIO-RK database [38] and saved into a JSON file.
5. The JSON files from BRENDA and SABIO-RK were merged into a combined JSON database.
6. The model reactions were mapped to their turnover numbers using the EC numbers.
7. The molecular weights of model proteins were calculated from their aminoacidic sequence, and mapped to their Uniprot ID.
8. The XLSX files for setting protein pool, enzyme concentrations, and enzyme stoichiometries were created [25]. The format of enzyme

stoichiometries was modified to make them available for the successive step.

9. The enzyme-constrained model was created using the "create_smoment_model_reaction_wise_with_sbml" function.

2.4. Model calibration

To improve their prediction capability, genome scale models need calibration of their parameters, in particular the upper limit of the protein pool and the turnover numbers.

The initial value of the protein pool was set to 0.095 g/gCDW, which was the value used to constrain the *Escherichia coli* enzyme constrained model *i*JO1366 * [26]. Then it was iteratively adjusted, to improve model simulation agreement with experimentally determined growth rates. In this phase, however, it was not possible to obtain a univocal value of protein pool that could allow good predictions of both autotrophic and heterotrophic growth. In fact, different enzyme pools had to be used to simulate different growth modes, resulting either in overestimation of autotrophic growth rates or underestimation of heterotrophic growth rates, as can be seen in Fig. 2. Thus, it was needed to first adjust the turnover rates.

The choice of the k_{cat}s to be adjusted has been carried out differently

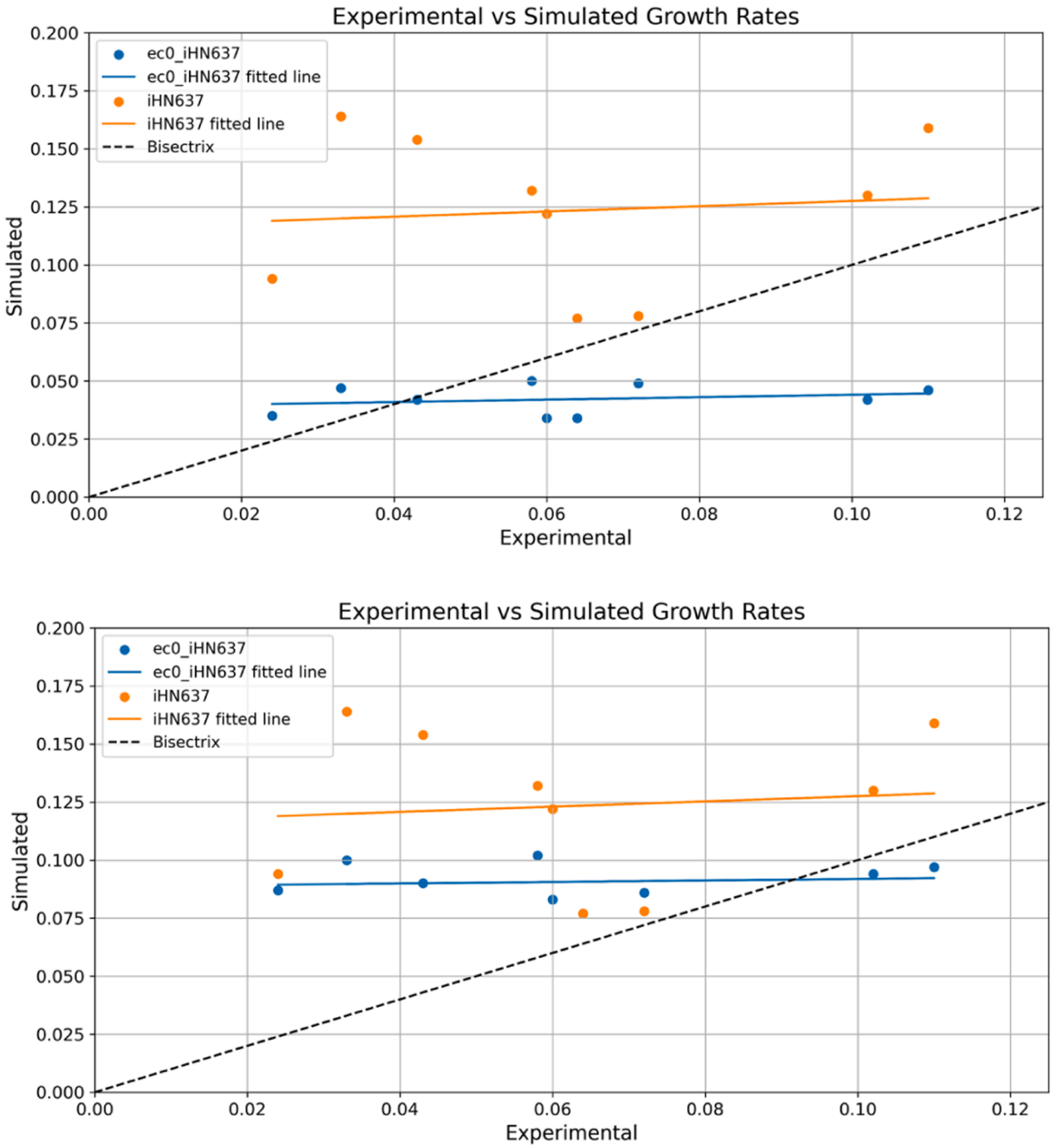

Fig. 2. Comparisons of model performance against experimental values at two different enzyme pool upper bounds, 0.03 g/gCDW (top figure) and 0.05 g/gCDW (bottom figure). Respectively, the first was giving a good fit for autotrophic growth with strong underestimation of the heterotrophic growth, the latter gave a good fit of growth rates on fructose with overestimation of autotrophic growth.

in previous studies, choosing reactions with high impact on simulation results [26] or reactions with high enzyme usage [28]. In this case, we chose to select for calibration the reaction's main high fluxes carrying reactions for different conditions (Table 1). For this reason, FBA simulations were performed using the EC model in different growth conditions, autotrophic and heterotrophic, constraining the substrates (CO and fructose) uptake rates respectively to 40 mmol/gCDW/h and 1.8 mmol/gCDW/h, which are fluxes close to experimental values measured for this strain. The main reactions identified were mainly glycolysis and WLP reactions. It has been previously demonstrated that *in vivo* determined k_{cat}s should be preferred, when available, to *in vitro* determined values, which are available on databases as BRENDA and SABIO-RK, used in autopacmen workflow [39]. In this case, it was possible to find in literature *in vivo* measured apparent turnover rates of *Clostridium autoethanogenum*, an acetogenic species closely related to *C. ljungdahlii* [40].

Thus, the selection of the turnover numbers to be adjusted was done by comparing, for the high fluxes carrying reactions, the k_{cat}s assigned by autopacmen with the *in vivo* values, and to *in silico* turnover numbers calculated using DLKcat, a Python-based deep learning tool able to predict the turnover rate of an enzyme based on its aminoacidic sequence and substrate [41]. Reactions selected for the calibration were those for which the previously assigned k_{cat} had strong deviations from the *in vivo* and the *in silico* value; for each of them, the k_{cat} was then substituted with the highest turnover number among the *in silico* and *in vivo* value. In Table 1 are indicated the reactions selected for k_{cat} calibration. In can be observed that in most cases, this step consisted in decreasing the turnover numbers of Wood-Ljungdahl Pathway related reaction. This may seem in contrast with what is usually observed during calibration of constrained models, in which the main issue is represented by avoiding over-constraining of the model [28,42]. However, this step allowed to reduce the overestimation of the strain metabolism during autotrophic growth, which characterized the original model and the first version of the updated model.

Then, it was possible to find an optimal value of the protein pool. Initially, a manual adjustment was performed to identify a range around the optimal protein pool value, starting again from the value of 0.095 g/gCDW. The optimal protein pool was then selected as the value minimizing the error with respect to experimental values using [26]:

$$E_{norm} = \left\| \frac{\mu_{sim} - \mu_{exp}}{\mu_{exp}} \right\| \quad (4)$$

2.5. Evaluation of prediction accuracy

The prediction accuracy of the generated enzyme-constrained model was evaluated by measuring the Pearson correlation coefficient, and by linear regression.

The experimental product profiles in the different conditions were also compared to the predictions by iHN637 and ec_iHN637.

Table 1
Updated turnover rates.

Reaction	k_{cat} assigned (s^{-1})	New k_{cat} (s^{-1})
CODH4	1787.21	73.85
CODH_ACS	250.79	70.71
FTHFLi	286.36	29.45
MTHFC_TG_reverse	896.68	48.16
ACKr_TG_reverse	1536.86	43.88
R_ALCD2x_TG_reverse	368.84	16.33
PTAr_TG_forward	1661.54	19.91
FRNDPR2r_TG_forward	Not assigned	15.15
MTHFR5_TG_forward	Not assigned	24.39
FDH7_TG_forward	Not assigned	84.75

2.6. Simulations

Simulations of the bacterium steady-state growth, by Flux balance analysis (FBA), were carried out using Cobrapy [43]. For computational design of metabolic interventions, it was used the package StrainDesign [44].

2.7. Bacterial growth conditions

C. ljungdahlii mixotrophic cultivations were carried out to retrieve data about growth rate, uptake, and secretion fluxes during simultaneous CO_2, H_2, and fructose consumption. This information is not available in the literature and was considered important for the determination of model performance.

C. ljungdahlii (DSM 13528) was ordered from the Leibniz Institute DSMZ – German Collection of Microorganisms and Cell Cultures GmbH [45]. The bacterium was grown anaerobically in 125 mL serum bottles containing 42 mL of modified DSM 879 medium [46], at 37 °C. In all cultivation experiments, the use of $NaHCO_3$ was avoided, and MES 50 mM was used as buffer; Sodium sulfide nonahydrate (Na_2S x 9 H_2O) was substituted by doubling the amount of Cysteine hydrochloride monohydrate (L-Cys HCl x H_2O) suggested in the medium recipe DSM 879. The gas mixture of 80% N_2: 20% CO_2 indicated in the medium recipe was also substituted by a mixture of 80% H_2: 20% CO_2. All bottles were pressurized once, before the start of the fermentation experiments, to a pressure of 2.5 bar. Two different fructose concentrations were tested, 5 g/L and 10 g/L. All experiments were performed in triplicates and compared to negative controls. The bottles were inoculated using 3 mL of inoculum from cultures in the mid-exponential growth phase (OD_{600} 0.5–0.8) Samples were collected shortly after inoculation and then every 24 h of the culture for determination of OD_{600}, pH, and metabolites concentrations. Before each sampling, the internal pressure of the bottles was measured, using a manometer connected to a needle, puncturing the butyl stopper of each bottle.

2.8. Detection of metabolites by HPLC

For the detection of metabolites of interest (fructose, acetic acid, ethanol), samples were centrifuged for 10 min at 4 °C, and filtrated with 0.22 μm syringe filters. The filtrated samples were analyzed using a Dionex Ultimate 3000 high-performance liquid chromatograph UHPLC+ focused system (Dionex Softron GmbH, Germering, Germany) equipped with a Bio-Rad Aminex HPX 87-H column, at 60 °C, using mM H_2SO_4 as mobile phase at a flowrate of 0.6 mL/min.

3. Results

3.1. The enzyme-constrained model ec_iHN637

The original model, iHN637, is characterized by a total of 785 reactions, and 698 metabolites [29]. In the enzyme-constrained model ec_iHN637, the number of reactions was increased to 956, due to the splitting of enzyme-catalyzed reversible reactions and the addition of the protein pool pseudo-reaction, while the number of metabolites was increased to 699 with the addition of the protein pool pseudo-metabolite.

Starting from 0.095 g/gCDW, the protein pool was manually decreased and an ideal range between 0.072 and 0.080 g/gCDW was identified. The final value of the protein pool was then set to 0.078 g/gCDW by minimizing the normalized error.

3.2. Evaluation of model growth rate prediction performance

The model performance was compared to the original metabolic model, iHN637, by evaluating the ability to predict growth rate, constraining the model with uptake rates obtained from the literature. Fig. 3

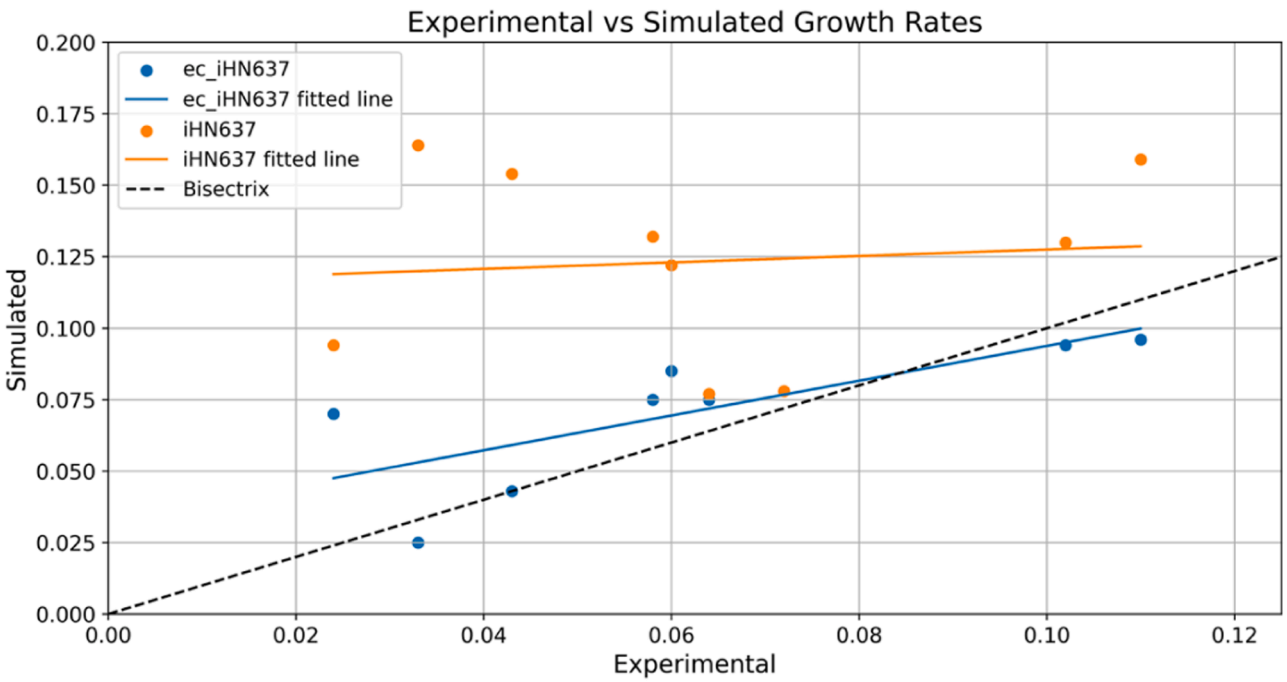

Fig. 3. Models' predictions accuracies. Comparison of accuracy of growth rate prediction between the original model iHN637 and the enzyme constrained ec_iHN637. When only one simulated value corresponds to an experimental one, the prediction by the original and the enzyme-constrained model were corresponding.

presents a comparison of the 2 models, showing that the prediction ability of growth rates was increased in the enzyme-constrained model. The plot was generated by comparing experimentally determined growth rates and simulated growth rates, from simulations in which only the uptake rates of substrates (CO_2, H_2, fructose, and CO) were used as constraints.

The data in Table 2 were used as constraints for the FBA simulations. The mean normalized error decreased from 1.42 for the original model to 0.37 in the enzyme-constrained model, with standard deviations equal to 1.41 and 0.59, respectively. The good correlation of the EC model with the *in vivo* growth rates was also evidenced by the results of Pearson's r, which was increased to 0.750 ($p = 0.020$), compared with the value of 0.096 ($p = 0.803$) for the original model. The result can be also compared to those obtained by the ME-model iJL965-ME, published in 2019, that had a Pearsońs r equal to 0.68 with a p value of 0.14 [30].

3.3. Effect of enzyme constraints and prediction of product fluxes

To visualize the effects of enzymatic constraints on the predictions of the model, the growth rates and production rates of acetate and ethanol were plotted for both the original model and the enzyme-constrained model (Figs. 4 and 5).

Table 2
Substrate fluxes constrained for FBA simulations for evaluation of the accuracy of growth rate prediction by the models.

Constrained Fluxes	Uptake rates [mmol/gCDW/h]	Growth rate [h^{-1}]	Source
H_2, CO	-7.724, – 40.132	0.043	[11]
H_2	-79.5	0.033	[12]
H_2, CO_2	-46.630, – 21.765	0.024	[11]
CO	-38.5	0.058	[12]
CO	-35.878	0.060	[11]
Fructose	-1.88	0.72	[29]
Fructose, CO_2	-0.672, – 15.861	0.110	[This study]
Fructose, CO_2	-0.615, – 16.480	0.102	[This study]
Fructose, CO_2	-0.507, – 8.785	0.064	[This study]

Growth on CO as substrate was simulated in the range 0–50 mmol/gCDW/h, considering that the experimental uptake rates found in the literature were 38.5 and 35.9 mmol/gCDW/h for the cases of growth on sole CO, while for the case of syngas fermentation an average uptake flux of 40.132 was reported [11,12]. Moreover, the maximum specific uptake rate of CO by *C. ljungdahlii* has been determined to be 34.4 mmol/gCDW/h utilizing a kinetic model [47].

For the iHN637 model, a continuous linear correlation was observed between the CO-specific uptake and the predicted growth rate during growth on CO. On the contrary, the ec_iHN637 model predicted a critical point, occurring between 20 and 30 mmol/gCDW/h, at which the enzyme pool reached its upper limit, interrupting the linear relationship between growth rate and CO uptake. The behavior is an effect of the introduction of the enzyme constraint in the model. Consequently, the iHN637 model did not forecast the onset of ethanol production when the model was constrained solely with uptake fluxes. Instead, Flux Balance Analysis (FBA) simulation predicted a steadily increasing production of acetate. In metabolic models, indeed, alternative fermentation products are not predicted, unless additional constraints are provided, on the secretion fluxes or the redox fluxes [30]. In the ec_iHN637, when the critical CO uptake flux was reached, the beginning of ethanol production was predicted as an overflow metabolism strategy to balance reducing equivalents. Despite the prediction of ethanol as the main fermentation product, comparing the results to the experimental values, the predictions by the ec_iHN637 model was still underestimating the ethanol production rate in the case of CO growth, and overestimating it in the case of syngas fermentation. In one of the experimental sources, also BDO and lactate production were observed [11], but none of the models was able to predict their secretion.

When the modes were used to simulate growth on syngas at different CO uptakes, leaving unconstrained the hydrogen uptake flux, the model iHN637 predicted a linear increase of growth rate at increasing uptake fluxes of CO (Fig. 5). In the enzyme constrained model, instead, a first interruption of the linear relationship was observed at 14 mmol/gCDW/h. In correspondence of this point, the model predicted a decrease of ethanol productivity and the start of emissions of CO_2. In the original model, instead, the absence of enzyme limitations allowed the model to

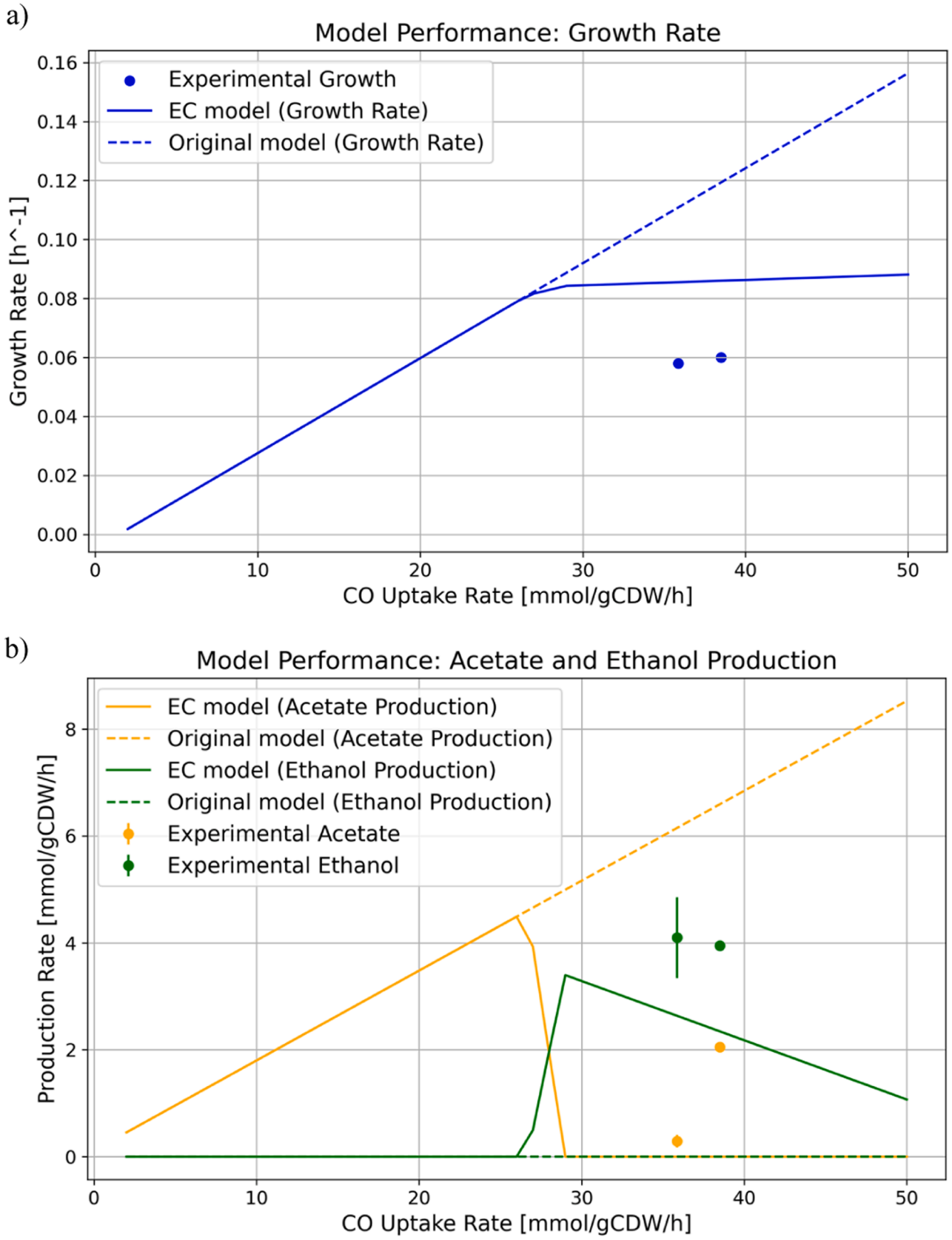

Fig. 4. Growth rate (a), acetate, and ethanol production (b) trends at increasing CO-specific uptake rates for growth on sole CO as substrate.

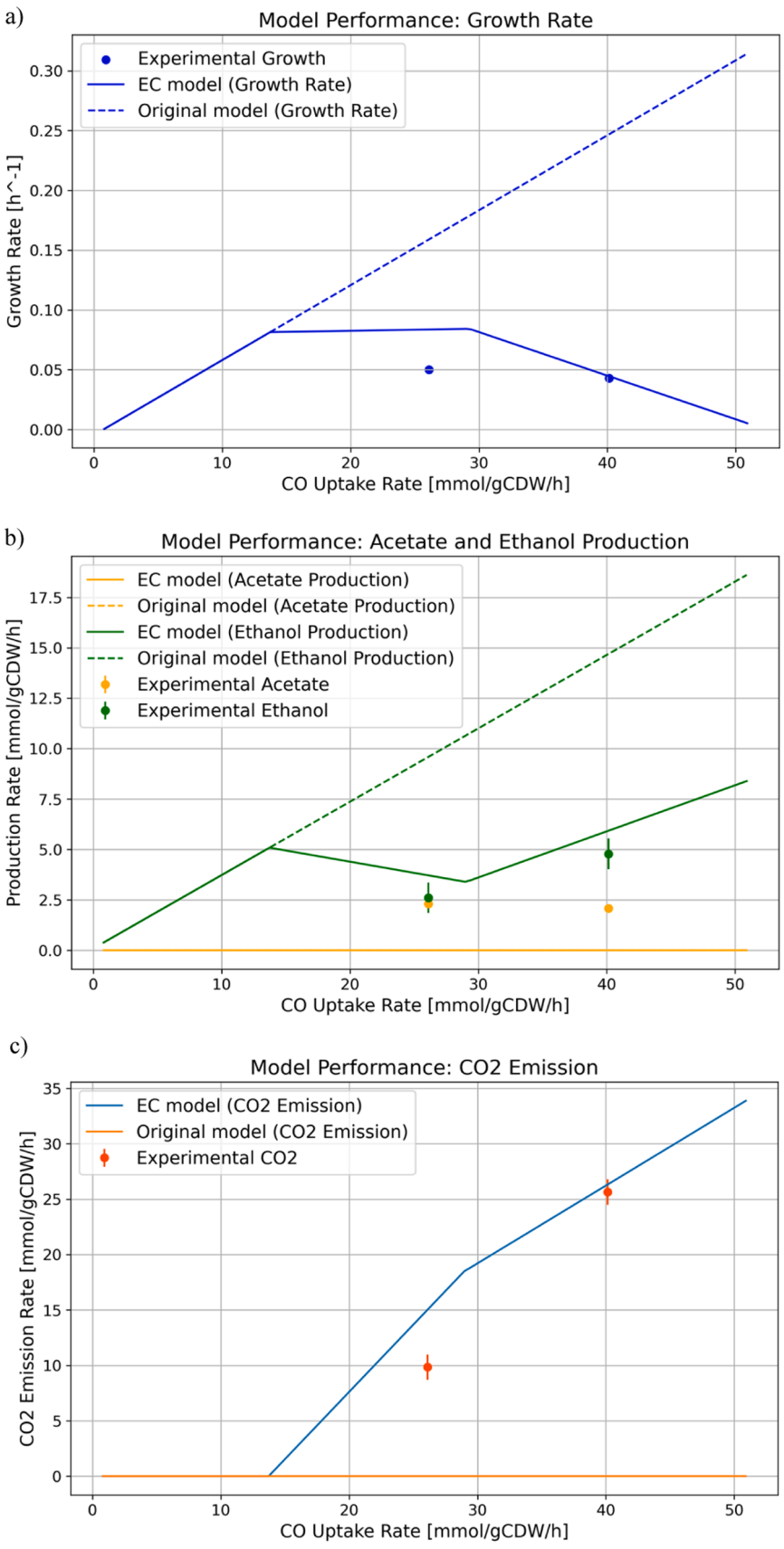

Fig. 5. Growth rate (a), acetate, and ethanol production (b), and CO_2 emissions (c) trends at increasing CO-specific uptake rates for growth on syngas ($CO+H_2$).

predict continuous increase of the growth and ethanol production, without emissions of CO_2, as all the carbon was directed into the metabolic pathways for production of biomass and ethanol. At CO uptake of 29 mmol/gCDW/h, the predictions by ec_iHN637 had showed another inflection point, corresponding to a decrease of growth rate and an increase of ethanol production. When compared to experimental points derived from literature [11,48], the enzyme constrained model showed again improved capability of predicting growth rate and exchange fluxes with respect to the original model.

When the model was constrained with CO_2 and fructose uptake, the range 25–80 mmol/gCDW/h of H_2 uptake rates was analyzed to simulate the mixotrophic conditions, with a minimum CO_2 uptake of 15.861 mmol/gCDW/h (Fig. 6).

In this scenario, the experimental values were not included in the graphs, since the experimental H_2 uptake flux was not known. The outcomes indicated that in this case, the two models, ec_iHN637 and iHN637, demonstrated less divergence in their trends compared to the case with CO, particularly concerning acetate and ethanol production. A notable difference, however, was seen in the maximum growth rate predictions at different H_2 uptake rates: the ec_iHN637 model predicted a maximum growth rate at 33.58 mmol/gCDW/h, while the iHN637 model predicted it at 48.34 mmol/gCDW/h. Thus, when the model was constrained without specifying the (unknown) H_2 uptake flux, the iHN637 model predicted a growth rate of 0.114 h^{-1} while in ec_iHN637 it was limited by the additional constraint to 0.094 h^{-1}, compared to an experimental value of 0.110. While the original iHN637 model's prediction was closer to the experimental value in this context, the divergence in product secretion rates was significant. The enzyme-constrained model was able to predict that acetate was nearly the sole secreted product, with a flux equal to 7.67 mmol/gCDW/h, compared to an experimental value of 6.79 mmol/gCDW/h. The model iHN637 predicted instead ethanol to be the only fermentation product, with a secretion rate equal to 7.47 mmol/gCDW/h, largely deviating from the experimental value of 0.0035 mmol/gCDW/h. The specific rate of ethanol production predicted by ec_iHN637 was equal to 0.245 mmol/gCDW/h.

3.4. *In silico metabolic engineering*

The new model was then used to predict potential genetic engineering to target and improve the secretion of metabolites of interest, from the perspective of an industrial application of the bacterium. The *in silico* engineering experiments were carried out constraining the model with substrate uptake fluxes simulating syngas fermentation and H_2-enhanced mixotrophy scenarios, as these are of particular interest for future industrial applications of the microorganism. It was decided to focus only on native products of C. *ljungdahlii,* since introduction of heterologous pathway for production of other metabolites (butyrate, butanol, acetone) would result in a strong burden for the cell. Production of native metabolites was thus considered a more feasible and realistic scenario.

3.4.1. *Metabolic engineering using syngas as substrate*

Syngas can be derived by the gasification of many different carbon-rich sources, including biomass [49], and its composition is influenced by feedstock characteristics and process conditions applied during gasification. In the present study, the model was constrained with the substrate fluxes from Hermann M. et al. [11] for syngas growth scenario, which were derived by the exponential growth of a batch culture *C. ljungdahlii* cultivated using a substrate with the following composition: 55% CO, 30% H_2, 5% CO_2, 10% Ar. A 25% possible variability of each constraint was also considered for the OptKnock simulations, in order to account for some variability of uptake rates when compared to other sources in literature [47,50] and possible minor adjustments of some fluxes.

The growth rate predicted by the FBA simulation in this condition was 0.068 h^{-1}, with an ethanol secretion flux of 4.83 mmol/gCDW/h, and CO_2 emission of 17.48 mmol/gCDW/h.

For OptFlux prediction of optimal knockouts, some parameters must be specified:

- The minimum growth rate to be reached by the mutant strains generated was set to 0.034 h^{-1}, half of the wild-type case.
- The minimum secretion flux for the desired product was different for each product.
- The maximum number of genetic interventions was limited to 3.

For the case of syngas fermentation, acetate overproduction was not considered, as any attempt to overproduce acetate would result in low acetate flux and negatively affected growth rates. Since the wild-type *C. ljungdahlii* grown using syngas as substrate was already producing mainly ethanol, production of a less reduced end product, such as acetic acid, would have negative effects on the growth of the bacterium, because of the impossibility to keep the redox state of the cell. Therefore, it was chosen to focus only on ethanol, lactate, and BDO production.

3.4.1.1. Ethanol production. For ethanol, the lower bound of ethanol secretion was set to 5.00 mmol/gCDW/h. The highest increase of ethanol secretion was reached when the number of knockouts was set to 3: the deletion of the reactions ACALD, PTAr, and LDH resulted in a 17.4% increase of the ethanol flux to 5.67 mmol/gCDW/h, with a growth rate reduced to 0.047 h^{-1}. No other products were predicted in the simulations (Table 3).

For all the predicted phenotypes displayed, there was an important trade-off between increased ethanol production and growth rate decrease which impacts the economy of such process when commercialized in industry. This is particularly relevant also if compared with results from previous OptKnock simulations on the original model iHN637 [50], in which predicted engineering strategies for iHN637 resulted in doubled ethanol flux compared to the wild-type, with a growth rate higher than 0.05 h^{-1}. In the present case, considering enzyme constraints to the model strongly inhibited the redirection of carbon and reducing equivalents towards ethanol production. Considering the analysis, it could be inferred that the wild-type strain is already optimized for ethanol production in the chosen scenario, given that ethanol is its sole product. Consequently, any potential improvement in its performance would likely stem from engineering strategies that enable the strain to enhance its uptake fluxes.

3.4.1.2. Lactate production. For lactate production, the minimum secretion rate was set to 5.00 mmol/gCDW/h. OptKnock was not able to predict any possible engineering strategy to increase the lactate secretion over this threshold with only one knockout, so only the results for the cases of two and three deletions are shown. In both cases, lactate was the only product predicted (Table 3).

In this case, the deletion strategies predicted by OptKnock resulted in lactate production not observed in the wild type, with a 33.8% decrease in growth rate for the case of 3 deletions, and a slightly lower decrease of 29.4% in the case of 2 deletions. The suggested strategy aims at the interruption of the pathways responsible for acetate, by deletion of the Acetate kinase (ACKr) and ethanol production, by deletion of the acetaldehyde dehydrogenase (ACALD). The FBA simulations for the mutant strains also showed decreased CO_2 emission fluxes, due to the increased need for carbon atoms for lactate production.

3.4.1.3. BDO production. For 2,3-butanediol production a minimum secretion flux of 3 mmol/gCDW/h was considered, as no mutant with fewer than 3 knockouts could reach higher thresholds (Table 3).

BDO production was predicted only for the case of 3 reaction knockouts, and as for other products, it was predicted to be the sole secretion by the cell, together with CO_2, in the simulated phenotype. The

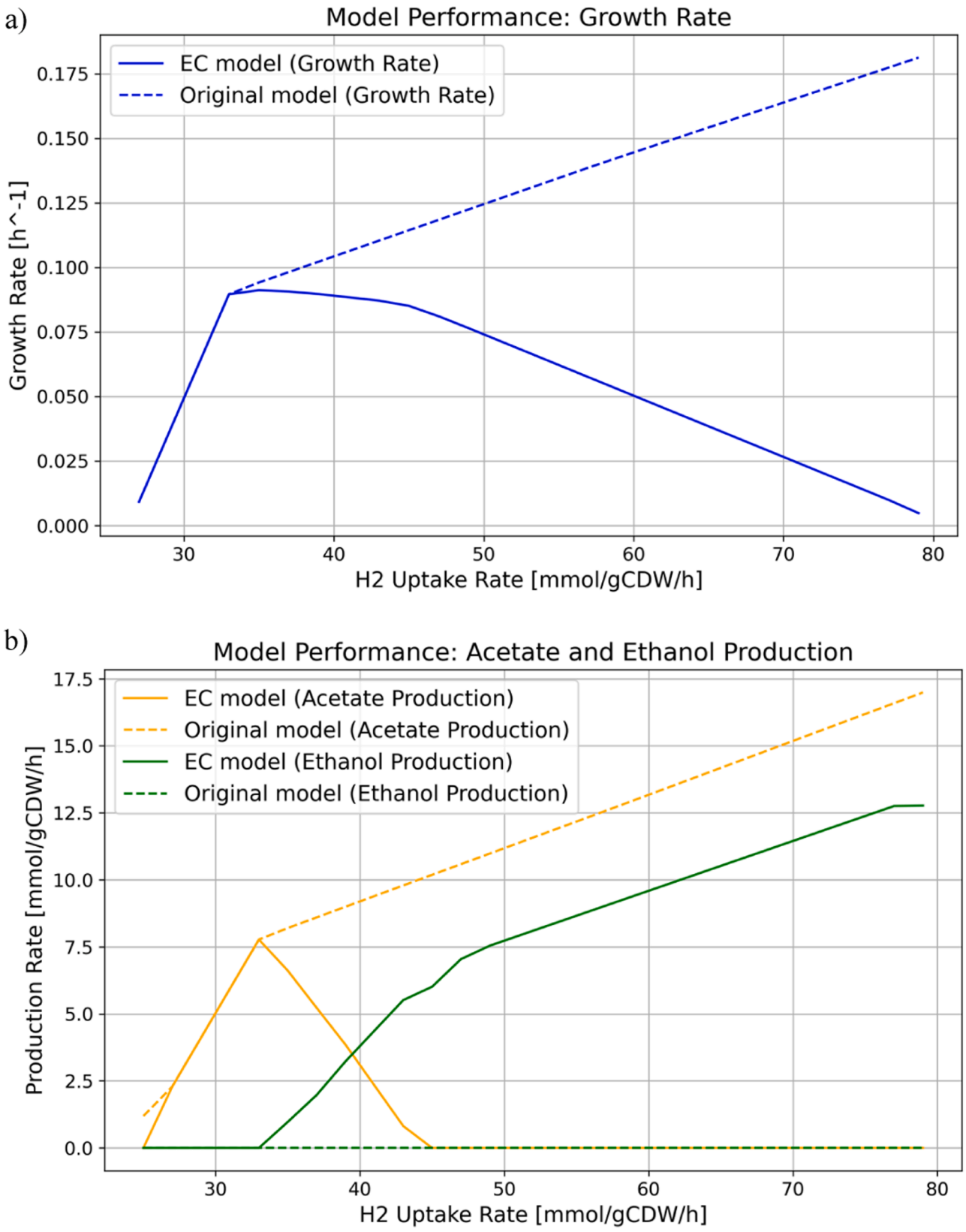

Fig. 6. Growth rates (a) and product fluxes (b) under mixotrophic growth. Growth rate, acetate, and ethanol production trend at increasing specific uptake rates of H_2.

Tablee 3
Knockout strategies for overproduction of Ethanol, Lactate and 2,3 Butanediol on syngas predicted by OptKnock with 1, 2, and 3 deletions, compared to wild type. In parenthesis is reported the % variation with respect to the wild type.

Desired product	Target reactions	Growth rate (h^{-1})	Product flux (mmol/gCDW/h)	CO_2 emission flux (mmol/gCDW/h)
Ethanol	Wild type	0.068	4.83	17.48
	KAS15	0.052 (−23.5%)	5.07 (+5.0%)	17.62 (+0.8%)
	KAS15, RNDR1	0.050 (−26.5%)	5.13 (+6.2%)	17.65 (+1.0%)
	ACALD, PTAr, LDH	0.047 (−30.9%)	5.67 (+17.4%)	19.61 (+12.2%)
Lactate	Wild type	0.068	0	17.48
	ACALD, ACKr	0.048 (- 29.4%)	5.77	14.31 (−18.1%)
	ACALD, ACKr, GLUDy	0.045 (−33.8%)	5.91	14.59 (−16.5%)
2,3 Butanediol	Wild type	0.068	0	17.48
	LDH, ACKr, ALCD2x	0.036 (−47.1%)	3.50	20.82 (+19.1%)

growth rate was strongly affected, with a 47.1% decrease, which brings the mutant growth rate very close to the threshold set for the strain. This was also the product for which the highest CO_2 fluxes were produced, as a result of the higher number of reducing equivalents needed for its production.

3.4.2. *Metabolic engineering in mixotrophic growth*

To simulate mixotrophic growth in OptKnock, the uptake fluxes of fructose, hydrogen, and carbon dioxide were constrained using values obtained for one of the mixotrophic cultures utilized in this study: 0.672 mmol/gCDW/h for fructose uptake, 33.6 mmol/gCDW/h for H_2 uptake, value that was obtained from previous FBA simulations.

The CO_2 flux was not constrained in order to be able to predict increases in CO_2 fixation that could result in some engineering strategies. The CO_2 uptake, however, is strongly correlated to electron availability, limited by the constraint on the maximum uptake of H_2, thus only moderate increases of CO_2 fixation could be predicted.

For the case of mixotrophic growth, only the overproduction of acetate and ethanol was considered, since no metabolic engineering strategy predicted by OptFlux was able to predict significant production of lactate and BDO while simultaneously utilizing H_2, CO_2, and fructose at the specified substrate uptakes.

The growth rate predicted by the FBA simulation in this condition was 0.093 h^{-1}, with acetate as the main product (6.92 mmol/gCDW/h) and ethanol secretion flux of 0.76 mmol/gCDW/h; in this case, CO_2 was consumed at a rate equal to 15.36 mmol/gCDW/h.

The OptFlux simulations were carried out as for the previous case with syngas, only increasing the constraint of minimal growth rate to 0.047 h^{-1}, half of the wild type.

3.4.2.1. Acetate production. For acetate overproduction, a minimum acetate secretion flux of 8 mmol/gCDW/h was used to constrain OptKnock. Some possible engineering strategies were identified with 1, 2, or 3 deletions, for increasing the specific flux of acetate, but in all cases, the increased secretion fluxes (22.3%, 25.6% and 29.9% respectively for 1, 2, and 3 deletions) also corresponded to strongly decreased growth rates (19.3%, 26.9% and 49.5%). The CO_2 fixation fluxes were also predicted to slightly increase, as a result of the increased availability of reducing equivalents generated by the reduced biomass formation (Table 4).

3.4.2.2. Ethanol production. For ethanol overproduction, the minimum secretion flux was set to 6 mmol/gCDW/h (Table 4). Also, for ethanol production, it was possible to reach the desired minimum rate of production considering only 1 deletion. The growth rate was strongly affected by the switch of production from acetogenic to solventogenic, for the reduced ATP gain caused by deletions of a key enzyme for acetate production, ACKr. Moreover, the CO_2 fixation was also strongly decreased with respect to the wild-type and acetate-producing strains, as a result of the decreased availability of reducing equivalents, which were diverted towards ethanol formation.

4. Discussion

Inclusion of enzyme constraints in metabolic models of microorganisms has been shown to strongly increase the ability to predict both wild-type and mutant phenotypes [24,26,42,51,52], thanks to the restriction of the flux distribution space. In the case of *C. ljungdahlii* introduction of enzyme constraints by sMOMENT workflow resulted in an improved performance in the prediction of growth rate and main secretion fluxes of the cell. In particular, the limitation in the maximum amount of metabolic enzyme present in the cells allowed to avoid overestimations of growth rates when compared to experimentally obtained values, for all the conditions tested. Also, the prediction of the product profile was much closer to actual values, with prediction of overflow metabolism during growth on CO, and the secretion of acetate as the main end product in mixotrophic conditions, differently from the original metabolic model. Further improvements in the prediction ability of the model can be reached by improvement of the k_{cat}s data utilized for the calculation of the enzyme costs. Availability of high-quality turnover rates data is indeed the key parameter in the construction of enzyme-constrained models [39], but for most of the strains, it is not possible to retrieve publicly available specific data. In the present study, most of the utilized enzymes were taken from web databases, BRENDA and SABIO-RK, where mainly *in vitro* k_{cat}s are available. Generation of strain-specific *in vivo* turnover rates, by coupling of FBA and proteomics, could further increase the prediction ability of the model [53,54]. *In vivo* inferred values of turnover rates available for *C. autoethanogenum* [40] were already used in the calibration of the present model.

Table 4
Knockout strategies for overproduction of acetate and ethanol in mixotrophic growth predicted by OptKnock with 1,2, and 3 deletions, compared to wild type. In parenthesis is reported the % variation with respect to the wild type.

Desired product	Target reactions	Growth rate (h^{-1})	Product flux (mmol/gCDW/h)	CO_2 fixation flux (mmol/gCDW/h)
Acetate	Wild type	0.093	6.92	15.36
	FRNDPR2r	0.075 (−19.3%)	8.51 (+23.0%)	16.24 (+5.7%)
	FBA, FRNDPR2r	0.068 (−26.9%)	8.69 (+25.6%)	16.30 (+6.1%)
	GHMT2r, ENO, FRNDPR2r	0.052 (−49.5%)	8.99 (+29.9%)	16.27 (+6.9%)
Ethanol	Wild type	0.93	0.76	15.36
	ACKr	0.053 (−43.0%)	6.04 (+695%)	10.36 (−32.6%)
	GLUDy, ACKr	0.049 (−47.3%)	6.11 (+704%)	10.32 (−32.8%)
	PSP_L, GLUDy, ACKr	0.047 (−49.7%)	6.14 (+708%)	10.30 (−32.9%)

An important application of metabolic models is the prediction of metabolic engineering interventions to improve the production of a desired metabolite, under specified growth conditions. Utilization of OptKnock through the StrainDesign package available on GitHub [44,55] allowed to design *in silico* mutant strains for potential syngas fermentation to ethanol, lactate, and BDO, which are native products of *C. ljungdahlii*. Despite many attempts to genetically engineer this strain aimed at the production of non-native metabolites by the introduction of heterologous pathways [10,15], these products were not included in the analysis, as enzyme kinetics were not available, and, most importantly, the introduction of heterologous pathways may represent too great a burden for the growth of these bacteria.

With respect to previous *in silico* analysis of possible mutant *C. ljungdahlii* strains, utilization of an enzyme constrained model did not result in redundant engineering strategies for overproduction of different metabolites [50]. The enzyme constrained model provided more reliable predictions of the growth rate and production fluxes with respect to the original model, and the performance of the generated overproducing mutants was negatively affected, due to the lower growth rates predicted by the enzyme-constrained model. In many cases, low increases in production fluxes corresponded to strong effects on the growth rate, which would discourage the application of the strain for industrial production. Mixotrophic metabolism of *C. ljungdahlii,* however, may offer some solutions to improve the metabolism of the strain, as already suggested in the literature [10,31,32]. In particular, when the model was constrained with experimental uptake fluxes, the mutants generated in mixotrophic conditions were able to produce acetate and ethanol while converting exogenous CO_2. Moreover, comparing the ethanol overproducing strains in syngas fermentation and mixotrophy, the latter were able to secrete higher fluxes, at higher growth rates, and simultaneously converting CO_2.

5. Conclusions

Recent developments in computational tools for synthetic biology may provide a great opportunity to improve the knowledge of acetogenic metabolism and to simulate potential metabolic engineering strategies to increase their industrial potential. An enzyme-constrained model for *in silico* simulation of *C. ljungdahlii* was generated utilizing the short MOMENT approach, resulting in a model with enhanced prediction capacity for the microbial phenotype under all conditions where experimental values were either retrieved from literature or generated in the lab. This model was subsequently utilized to simulate knockout strategies aimed at increasing the production of valuable native metabolites, using the OptKnock computational framework. In the context of syngas fermentation, strains engineered for overproduction of ethanol and BDO demonstrated a reduced growth rate and an increased CO_2 emission per gram of cell dry weight. For lactic acid production, growth rate was negatively affected but CO_2 emissions were reduced with respect to the wild type. Simulated knockouts in the mixotrophic growth of *C. ljungdahlii* did not yield strains capable of producing lactic acid and BDO, given the parameters applied to OptKnock. However, this solution appears promising to produce acetic acid or ethanol, leading to higher growth rates and net uptake of CO_2 instead of emission. The practical feasibility of these strategies will need to be validated *in vivo*.

Author Agreement

We certify that all authors have seen and approved the final version of the manuscript being submitted. We also confirm that this is an original work that has not been published previously and that is not under consideration for publication elsewhere. All the authors agreed that this manuscript should be submitted to Computational and Structural Biotechnology Journal. If accepted for publication, it will not be published elsewhere in the same form, in English or any other language, including electronically, without the consent of the copyright holder.

Declaration of Competing Interest

The authors declare that they have no known competing financial interests or personal relationships that could have appeared to influence the work reported in this paper.

Acknowledgements

This work was supported by the Novo Nordisk Foundation (NNF), Denmark (grant number: NNF20SA0066233).

Appendix A. Supporting information

Supplementary data associated with this article can be found in the online version at doi:10.1016/j.csbj.2023.09.015.

References

[1] AR6 Synthesis Report: Climate Change 2023. https://www.ipcc.ch/report/ar6/syr/ (Accessed 06 June 2023).
[2] Mussatto SI, Yamakawa CK, van der Maas L, Dragone G. New trends in bioprocesses for lignocellulosic biomass and CO_2 utilization. Renew Sustain Energy Rev 2021;vol. 152:111620. https://doi.org/10.1016/J.RSER.2021.111620.
[3] Daneshvar E, Wicker RJ, Show PL, Bhatnagar A. Biologically-mediated carbon capture and utilization by microalgae towards sustainable CO_2 biofixation and biomass valorization – a review. Chem Eng J 2022;vol. 427:130884. https://doi.org/10.1016/J.CEJ.2021.130884.
[4] Fast AG, Papoutsakis ET. Stoichiometric and energetic analyses of non-photosynthetic CO_2-fixation pathways to support synthetic biology strategies for production of fuels and chemicals. Curr Opin Chem Eng 2012;vol. 1(4):380–95. https://doi.org/10.1016/J.COCHE.2012.07.005.
[5] Bar-Even A, Noor E, Milo R. A survey of carbon fixation pathways through a quantitative lens. J Exp Bot 2012;vol. 63(6):2325–42. https://doi.org/10.1093/JXB/ERR417.
[6] Ragsdale SW, Pierce E. Acetogenesis and the Wood-Ljungdahl pathway of CO_2 fixation. Biochim Et Biophys Acta - Proteins Proteom 2008;vol. 1784(12):1873–98. https://doi.org/10.1016/j.bbapap.2008.08.012.
[7] 'About – LanzaTech'. https://lanzatech.com/about/ (Accessed 13 June 2023).
[8] Liew FE, et al. Carbon-negative production of acetone and isopropanol by gas fermentation at industrial pilot scale. Nat Biotechnol 2022 40:3 2022;vol. 40(3):335–44. https://doi.org/10.1038/s41587-021-01195-w.
[9] Tanner RS, Miller LM, Yang D. Clostridium ljungdahlii sp. nov., an acetogenic species in clostridial rRNA homology group I. Int J Syst Bacteriol 1993;vol. 43(2):232–6. https://doi.org/10.1099/00207713-43-2-232.
[10] Jones SW, et al. CO 2 fixation by anaerobic non-photosynthetic mixotrophy for improved carbon conversion. Nat Commun 2016;vol. 7. https://doi.org/10.1038/ncomms12800.
[11] Hermann M, et al. Electron availability in CO_2, CO and H2 mixtures constrains flux distribution, energy management and product formation in Clostridium ljungdahlii. Micro Biotechnol 2020;vol. 13(6):1831–46. https://doi.org/10.1111/1751-7915.13625.
[12] J.R. Phillips, E.C. Clausen, and J.L. Gaddy, Synthesis Gas as Substrate for the Biological Production of Fuels and Chemicals'.
[13] Dahle ML, Papoutsakis ET, Antoniewicz MR. 13C-metabolic flux analysis of Clostridium ljungdahlii illuminates its core metabolism under mixotrophic culture conditions. Metab Eng 2022;vol. 72:161–70. https://doi.org/10.1016/J.YMBEN.2022.03.011.
[14] Köpke M, et al. Clostridium ljungdahlii represents a microbial production platform based on syngas. Proc Natl Acad Sci USA 2010;107(29):13087–92. https://doi.org/10.1073/pnas.1004716107.
[15] Pavan M, et al. Advances in systems metabolic engineering of autotrophic carbon oxide-fixing biocatalysts towards a circular economy. Metab Eng 2022;vol. 71:117–41. https://doi.org/10.1016/J.YMBEN.2022.01.015.
[16] O'Brien EJ, Monk JM, Palsson BO. Using genome-scale models to predict biological capabilities. Cell 2015;vol. 161(5):971–87. https://doi.org/10.1016/J.CELL.2015.05.019.
[17] Orth JD, Thiele I, Palsson BO. What is flux balance analysis? Nat Biotechnol 2010 28:3 2010;vol. 28(3):245–8. https://doi.org/10.1038/nbt.1614.
[18] Gu C, Kim GB, Kim WJ, Kim HU, Lee SY. Current status and applications of genome-scale metabolic models. Genome Biol 2019 20:1 2019;vol. 20(1):1–18. https://doi.org/10.1186/S13059-019-1730-3.
[19] Bi X, Liu Y, Li J, Du G, Lv X, Liu L. Construction of multiscale genome-scale metabolic models: frameworks and challenges. Biomol 2022, Vol 12, Page 721 2022;vol. 12(5):721. https://doi.org/10.3390/BIOM12050721.
[20] O'Brien EJ, Lerman JA, Chang RL, Hyduke DR, Palsson B. Genome-scale models of metabolism and gene expression extend and refine growth phenotype prediction. Mol Syst Biol 2013;vol. 9(1):693. https://doi.org/10.1038/MSB.2013.52.
[21] Lerman JA, et al. In silico method for modelling metabolism and gene product expression at genome scale. Nat Commun 2012 3:1 2012;vol. 3(1):1–10. https://doi.org/10.1038/ncomms1928.

[22] Saa PA, Nielsen LK. Formulation, construction and analysis of kinetic models of metabolism: a review of modelling frameworks. Biotechnol Adv 2017;vol. 35(8): 981–1003. https://doi.org/10.1016/J.BIOTECHADV.2017.09.005.
[23] Lu H, Kerkhoven EJ, Nielsen J. Multiscale models quantifying yeast physiology: towards a whole-cell model. Trends Biotechnol 2022;vol. 40(3):291–305. https://doi.org/10.1016/J.TIBTECH.2021.06.010.
[24] Domenzain I, et al. Reconstruction of a catalogue of genome-scale metabolic models with enzymatic constraints using GECKO 2.0. Nat Commun 2022 13:1 2022;vol. 13(1):1–13. https://doi.org/10.1038/s41467-022-31421-1.
[25] Orth JD, et al. A comprehensive genome-scale reconstruction of Escherichia coli metabolism–2011. Mol Syst Biol 2011;vol. 7. https://doi.org/10.1038/MSB.2011.65.
[26] Bekiaris PS, Klamt S. Automatic construction of metabolic models with enzyme constraints. BMC Bioinforma 2020;vol. 21(1):1–13. https://doi.org/10.1186/S12859-019-3329-9/TABLES/2.
[27] Sánchez BJ, Zhang C, Nilsson A, Lahtvee P-J, Kerkhoven EJ, Nielsen J. Improving the phenotype predictions of a yeast genome-scale metabolic model by incorporating enzymatic constraints. Mol Syst Biol 2017;vol. 13(8):935. https://doi.org/10.15252/MSB.20167411.
[28] Mao Z, et al. ECMpy, a simplified workflow for constructing enzymatic constrained metabolic network model. Biomolecules 2022;vol. 12(1):65. https://doi.org/10.3390/BIOM12010065/S1.
[29] Nagarajan H, Sahin M, Nogales J, Latif H, Lovley DR, Ebrahim A. Characterizing acetogenic metabolism using a genome-scale metabolic reconstruction of Clostridium ljungdahlii 2013;13(1).
[30] Liu JK, et al. Predicting proteome allocation, overflow metabolism, and metal requirements in a model acetogen. PLoS Comput Biol 2019;vol. 15(3). https://doi.org/10.1371/journal.pcbi.1006848.
[31] Fast AG, Schmidt ED, Jones SW, Tracy BP. Acetogenic mixotrophy: NOVEL options for yield improvement in biofuels and biochemicals production. Current Opinion in Biotechnology, vol. 33. Elsevier Ltd,; 2015. p. 60–72. https://doi.org/10.1016/j.copbio.2014.11.014.
[32] Maru BT, Munasinghe PC, Gilary H, Jones SW, Tracy BP. Fixation of CO_2 and CO on a diverse range of carbohydrates using anaerobic, non-photosynthetic mixotrophy. FEMS Microbiol Lett 2018;vol. 365(8). https://doi.org/10.1093/femsle/fny039.
[33] 'BiGG Models'. http://bigg.ucsd.edu/ (Accessed 25 April 2023).
[34] Lieven C, et al. MEMOTE for standardized genome-scale metabolic model testing. Nat Biotechnol 2020 38:3 2020;vol. 38(3):272–6. https://doi.org/10.1038/s41587-020-0446-y.
[35] 'Retrieve/ID mapping | UniProt'. https://www.uniprot.org/id-mapping (Accessed 01 May 2023).
[36] Cuevas DA, Edirisinghe J, Henry CS, Overbeek R, O'Connell TG, Edwards RA. From DNA to FBA: how to build your own genome-scale metabolic model. Front Microbiol 2016;vol. 7(JUN):907. https://doi.org/10.3389/FMICB.2016.00907/BIBTEX.
[37] 'BRENDA Enzyme Database'. https://www.brenda-enzymes.org/ (Accessed 01 May 2023).
[38] 'Search - Sabio-RK'. http://sabio.h-its.org/newSearch/index (Accessed 21 May 2023).
[39] Chen Y, Nielsen J. Mathematical modeling of proteome constraints within metabolism. Curr Opin Syst Biol 2021;vol. 25:50–6. https://doi.org/10.1016/J.COISB.2021.03.003.
[40] Valgepea K, et al. Absolute Proteome Quantification in the Gas-Fermenting Acetogen Clostridium autoethanogenum. mSystems 2022;vol. 7(2). https://doi.org/10.1128/MSYSTEMS.00026-22.
[41] Li F, et al. Deep learning-based kcat prediction enables improved enzyme-constrained model reconstruction. Nat Catal 2022 5:8 2022;vol. 5(8):662–72. https://doi.org/10.1038/s41929-022-00798-z.
[42] Wu K, et al. ecBSU1: a genome-scale enzyme-constrained model of bacillus subtilis based on the ECMpy workflow. Microorganisms 2023;vol. 11(1):178. https://doi.org/10.3390/MICROORGANISMS11010178/S1.
[43] A. Ebrahim, J.A. Lerman, B.O. Palsson, and D.R. Hyduke, COBRApy: COnstraints-Based Reconstruction and Analysis for Python, 2013. [Online]. Available: http://www.biomedcentral.com/1752–0509/7/74.
[44] Schneider P, Bekiaris PS, von Kamp A, Klamt S. StrainDesign: a comprehensive python package for computational design of metabolic networks. Bioinformatics 2022;vol. 38(21):4981–3. https://doi.org/10.1093/BIOINFORMATICS/BTAC632.
[45] 'German Collection of Microorganisms and Cell Cultures GmbH: Welcome to the Leibniz Institute DSMZ'. https://www.dsmz.de/ (Accessed 24 May 2023).
[46] '879: CLOSTRIDIUM LJUNGDAHLII MEDIUM, 2022.
[47] Mohammadi M, Mohamed AR, Najafpour GD, Younesi H, Uzir MH. Kinetic studies on fermentative production of biofuel from synthesis gas using clostridium ljungdahlii. Sci World J 2014;vol. 2014. https://doi.org/10.1155/2014/910590.
[48] Oliveira L, Rückel A, Nordgauer L, Schlumprecht P, Hutter E, Weuster-Botz D. Comparison of syngas-fermenting clostridia in stirred-tank bioreactors and the effects of varying syngas impurities. Microorganisms 2022;vol. 10(4). https://doi.org/10.3390/MICROORGANISMS10040681/S1.
[49] Molino A, Larocca V, Chianese S, Musmarra D. Biofuels production by biomass gasification: a review. Energ 2018, Vol 11, Page 811 2018;vol. 11(4):811. https://doi.org/10.3390/EN11040811.
[50] Chen J, Henson MA. In silico metabolic engineering of Clostridium ljungdahlii for synthesis gas fermentation. Metab Eng 2016;vol. 38:389–400. https://doi.org/10.1016/J.YMBEN.2016.10.002.
[51] Zhou J, Zhuang Y, Xia J. Integration of enzyme constraints in a genome-scale metabolic model of Aspergillus niger improves phenotype predictions. Micro Cell Fact 2021;vol. 20(1):1–16. https://doi.org/10.1186/S12934-021-01614-2/FIGURES/11.
[52] Massaiu I, et al. Integration of enzymatic data in Bacillus subtilis genome-scale metabolic model improves phenotype predictions and enables in silico design of poly-γ-glutamic acid production strains. Micro Cell Fact 2019;vol. 18(1):1–20. https://doi.org/10.1186/S12934-018-1052-2/FIGURES/8.
[53] Li Z, et al. High-throughput and reliable acquisition of in vivo turnover number fuels precise metabolic engineering. Synth Syst Biotechnol 2022;vol. 7(1):541–3. https://doi.org/10.1016/J.SYNBIO.2021.12.006.
[54] Davidi D, Milo R. Lessons on enzyme kinetics from quantitative proteomics. Curr Opin Biotechnol 2017;vol. 46:81–9. https://doi.org/10.1016/J.COPBIO.2017.02.007.
[55] Burgard AP, Pharkya P, Maranas CD. Optknock: a bilevel programming framework for identifying gene knockout strategies for microbial strain optimization. Biotechnol Bioeng 2003;vol. 84(6):647–57. https://doi.org/10.1002/BIT.10803.